Alteration of plagioclase and pyroxene phenocrysts in a fissure fumarole, Valley of Ten Thousand Smokes, Alaska

Michael N. Spilde, Adrian J. Brearley, James J. Papike

Institute of Meteoritics, Department of Earth and Planetary Sciences, University of New Mexico, Albuquerque, New Mexico 87131, U.S.A.

Abstract

The alteration of magmatic plagioclase and pyroxene phenocrysts in tephra adjacent to the conduit of a fissure fumarole from the Valley of Ten Thousand Smokes, Katmai, Alaska, was studied by electron microprobe and transmission electron microscopy. In slightly altered tephra, plagioclase compositions $>An_{73}$ are not observed, the more calcic portions of the phenocrysts having been replaced by amorphous silica. With increasing proximity to the fumarole conduit, progressively more sodic parts of the phenocrysts have disappeared. Adjacent to the fumarole, plagioclase $>An_{44}$ has been removed because of the increased solubility of albitic feldspar in chloride-rich solutions as a function of increasing temperature. On a submicrometer scale, a zonal sequence of replacement phases has developed at the interface between unaltered and altered feldspar. A thin leached surface layer (<500 Å), depleted in Al, Na, and Ca, but highly enriched in Si and Cl, is always present. In altered phenocrysts away from the vent, a zone ≤5000 Å of amorphous Al-bearing silica is present, locally containing secondary Al-rich smectite crystals. Closer to the fumarole, smectite is absent, and the zone of impure amorphous silica is much thinner. Extensive alteration of pyroxene phenocrysts only occurs close to the fumarole conduit, where replacement develops along fractures and parallel to (100). A narrow leached zone (200–300 Å), depleted in Mg and Ca, is present at the alteration interface, and halloysite is present locally as a secondary precipitate. The alteration of both plagioclase and pyroxene occurred when the fumarole system had cooled significantly (<300 °C) and was dominated by Si-rich, Cl-bearing aqueous fluids with pH < 2.5.

Introduction

The Valley of Ten Thousand Smokes (VTTS) and the Katmai volcanic system, Alaska, provide a unique geological laboratory for the study of a pristine volcanic system and associated fumarolic phenomena. The VTTS is particularly suited for the investigation of these fumarolic processes because extensive studies were conducted on the active fumaroles early in their history, shortly after the 1912 Katmai eruption (Shipley, 1920; Allen and Zies, 1923; Zies, 1929). More recent studies by Lovering (1957), Keith (1983, 1984, 1991a), Papike et al. (1991a, 1991b), and Papike (1992) have examined the alteration and mass transport associated with these fumaroles. The ability to examine the fumaroles in terms of gas content, temperature, and the deposition of minerals, particularly soluble compounds (early studies), and to return to reexamine the preserved fumaroles after cooling (later studies) provides valuable information about in situ vapor phase and hydrothermal alteration.

Our earlier studies (Papike et al., 1991a, 1991b; Papike, 1992) emphasized total bulk-sample mass flux of major, minor, and trace elements. This paper describes our first look at individual mineral alteration (plagioclase and pyroxene). Because bulk chemical transport is controlled by the reactions occurring between minerals and fluids within both source and depositional areas, the intent of this study is to provide some insight into the reactions that are occurring, at a submicrometer scale, within the chemical source area. To accomplish this, we have studied a cross-sectional suite of samples outward from a fumarolic vent conduit into unaltered tuff, which provides a complete sequence of altered to unaltered plagioclase and pyroxene phenocrysts and matrix glass. Two objectives of the study are, first, to quantify the onset of alteration under this specific set of natural conditions, and, second, to determine the reaction mechanisms that contributed to mineral alteration and the transportation mechanisms by which elements were moved into and out of the reaction zones within the individual phenocrysts.

The fumarole selected for this study is part of an extinct high-temperature fissure fumarole located in the middle valley of VTTS (see Fig. 1 of Papike, 1992, for the location of fumarole 212). The ash-flow deposit in VTTS ranges from a depth of a few meters in the lower valley 20 km from the vent to approximately 150–170 m in the middle valley, although the original pyroclastic deposit may have been nearly 200 m thick (Kienle, 1991). Hildreth (1983) describes the ash-flow deposit in detail. Several types of rootless fumaroles developed in the dacitic

ash-flow sheet and overlying air-fall layer immediately after eruption; their configuration and distribution was controlled by the degree of welding in the sheet, which in turn controlled fracturing and permeability (Keith, 1991a). Portions of the upper depositional region of the fumarole have been removed by erosion, exposing a vertical joint that served as a conduit for gases venting from the ash-flow sheet below. The vigorously rising, hot fluids leached and sintered the adjacent tuff in this part of the fumarolic system (Keith, 1991a). The elements leached from the lower portion of the fumarole system were deposited within a permeable ash fallout layer that overlies the welded ash-flow sheet. A detailed description of the upper portion of the fissure fumarole can be found in Keith (1991a), Papike et al. (1991b), and Papike (1992). Hydrothermal alteration of the dacitic tephra and minor andesitic pumice that make up the ash flow is superimposed on earlier fumarolic (vapor phase) alteration. Fumarole temperatures were as high as 645 °C, but most fumaroles died out within 30 yr (Keith, 1991b).

EXPERIMENTAL METHODS

Polished thin sections of tuff fragments that included fumarolic minerals were prepared for microprobe analysis. Doubly polished demountable thin sections of additional samples suitable for microprobe and TEM analysis were also prepared. Microprobe analysis and SEM observations were conducted on a Jeol 733 Superprobe equipped with a backscattered electron detector, five wavelength spectrometers, and a Tracor Northern 2000 energy-dispersive system. Analyses were conducted using standards of natural glass (basaltic glass USNM 113498/1, rhyolitic glass USNM 72854) and minerals (anorthite USNM 137041, anorthoclase USNM 133868, apatite USNM 104021, augite UNM A209, and scapolite USNM R6600-1); see Jarosewich et al. (1980) for the USNM standard compositions. To avoid Na and F diffusion within the sample during analysis, a beam diameter of 10–20 μm at a beam current of 10 nA was used for glass analyses; a beam diameter of 5–10 μm at 20 nA was used for plagioclase and a 1-μm beam at 20 nA for pyroxene. A Bence and Albee (1968) routine was used for correction of the microprobe data. After characterization by electron microprobe, pyroxene and plagioclase phenocrysts were removed from the thin section and were prepared for TEM examination by conventional ion-beam milling. The TEM studies were carried out with a Jeol 2000FX analytical transmission electron microscope operating at 200 kV. In situ quantitative energy-dispersive analyses were performed using a Tracor Northern 5500, and data reduction was accomplished by the Cliff-Lorimer thin film approximation (Cliff and Lorimer, 1975) using experimental k factors. The procedures and standards used for the k-factor determination are described in Mackinnon et al. (1986). Products of alteration reactions were identified by a combination of electron diffraction analysis, analytical electron microscopy, and high-resolution electron microscopy. Several phases were found that exhibit broad, diffuse diffraction rings in electron diffraction patterns. High-resolution TEM images of these phases show no evidence of short-range order, consistent with an aperiodic material. We refer to phases with these characteristics as amorphous throughout the paper. Bulk X-ray diffraction modal analyses were conducted on a Philips diffractometer using the reference intensity ratio method; see Papike et al. (1991b) for details of the method.

ELECTRON MICROPROBE/SEM STUDIES

Least altered sample

Samples J–O were taken sequentially outward from the fumarole vent wall toward less altered tuff (Fig. 1). The farthest from the fumarole and the least altered is sample 212O, taken at a distance of approximately 35 cm from the vent. The sample consists of essentially unaltered dacite with rare andesite pumice clasts. Euhedral and subhedral plagioclase phenocrysts in this sample are uncorroded and appear fresh. Plagioclase ranges in composition from An_{34} to An_{82} in this sample; zoning may cover an extensive range in a single phenocryst, from An_{80} in the core to An_{47} at the rim (Table 1, analyses 10 and 11). Hildreth (1983) determined that plagioclase in dacite pumice at Katmai ranges in composition from An_{34} to An_{71}, with An_{36}–An_{53} being the most common, but andesitic plagioclase is found with anorthite contents as high as An_{94}. The majority of phenocrysts in this study exhibit normal zoning, although reverse and oscillatory zoning are also common. In addition, both the feldspar and pyroxene phenocrysts often contain numerous inclusions of mineral and glass in their interiors. Pyroxene phenocrysts of hypersthene (Wo_3En_{30-40}) and augite ($Wo_{43-45}En_{15-20}$) are euhedral to subhedral, fresh, and unaltered. Pumiceous glass occurs as both scattered clean shards and as locally devitrified groundmass. The fresh shards are dacitic in composition ($SiO_2 \approx 68$ wt%), and slightly silica-rich in comparison with Hildreth's (1983) analysis of Katmai dacite, which ranges from 64.5 to 66 wt% SiO_2.

Altered samples

The remaining samples show increasing degrees of alteration inward toward the fissure. At 25 cm from the vent, most phenocrysts in 212N do not appear significantly different from those in 212O. However, calcic plagioclase phenocrysts in an andesite pumice clast manifest incipient alteration within their cores. These feldspars, the most calcic plagioclase found in this suite, exhibit only minor zoning from cores of about An_{87} (Table 1) to slightly more sodic rims and enclose original melt glass and pyroxene inclusions. The alteration occurs on the margin of the enclosed, devitrified glass and extends only a few micrometers into the plagioclase. Pyroxenes in this sample appear fresh and unaltered. Pumiceous glass is largely devitrified, but rare unaltered glass shards are present and have obvious alteration surrounding relict interiors.

Sample 212M was taken at approximately 15 cm from the fissure. Optically, feldspar phenocrysts begin to show
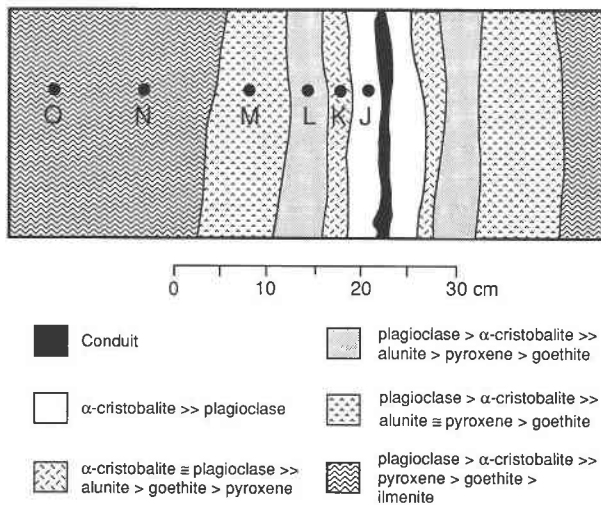
Fig. 1. Schematic map showing the location of samples J–O in dacite rich ash-flow tuff in the region of the fossil fumarole conduit. The relative abundance of the crystalline phases, as determined by optical petrography, in the nearly symmetric alteration zones adjacent to the conduit are noted. Encrusting minerals, characteristic of the upper surface region of the fissure fumaroles at Katmai, have been removed by erosion. (After Papike et al., 1991b.)

signs of incipient alteration in the form of patchy areas and zones of cloudiness. Microprobe analyses conducted in these areas exhibited low totals ($\approx$90–95 wt%); back-scattered electron (BSE) images indicate a network of irregular alteration too small to adequately probe without overlap onto adjacent unaltered feldspar. Large euhedral pyroxene crystals show no obvious sign of alteration, though small phenocrysts exhibit alteration around the

exterior and along internal fractures. Alteration of the pumiceous glass is pervasive, with no remaining fresh shards. Fibrous cristobalite commonly fills vesicles and, in some cases, appears to replace pumice clasts that are surrounded by rims of iron oxide.

In 212L, 10 cm from the fissure, plagioclase phenocrysts show significant signs of alteration. The feldspars in this sample, as in most of the altered samples 212J–N, exhibit varying degrees of alteration, depending on the Ca content of the plagioclase. Growth zones within the phenocrysts are either partially or completely replaced with dark Si-rich material throughout the crystal, and the most calcic feldspars are extensively replaced. Altered zones, a typical example shown in Figure 2, are only partially developed, leaving relicts of plagioclase large enough to be analyzed by electron microprobe (Table 1, analyses 6–8). As in the previous sample, only small pyroxene phenocrysts show evidence of alteration along rims and fractures. The groundmass is totally devitrified and coarser grained than previous samples; in many cases textures within pumice clasts have been eradicated.

At only 5 cm from the vent, in sample 212K, both plagioclase and pyroxene phenocrysts exhibit varying degrees of alteration. Incomplete replacement of growth zones in the feldspar once again allowed for quantitative microprobe analysis of relict feldspars (Fig. 3A). Plagioclase with compositions >An$_{55}$ has a tendency to be selectively corroded and may be completely replaced by amorphous silica, whereas slightly more sodic plagioclase (<An$_{51}$) survives untouched (Table 1, analyses 3–5). X-ray maps from an area of partially corroded feldspar indicate that both Ca and Al were removed (Fig. 3B, 3C) and replaced by Si-rich material with significant amounts of Cl, as high as 2 wt%. Small pyroxene crystals in this sam-

TABLE 1. Selected microprobe analyses of plagioclase phenocrysts

	1 212J	2 212J	3 212K	4 212K	5 212K	6 212L	7 212L	8 212L	9 212N	10 212O	11 212O
						Oxides (wt%)					
SiO$_2$	57.44	55.58	54.74	55.36	55.90	51.44	48.72	48.81	44.95	54.59	47.45
TiO$_2$	0.02	0.04	0.02	0.03	0.03	0.02	0.01	0.01	0.02	0.04	0.04
Al$_2$O$_3$	26.58	27.13	29.10	28.98	28.00	30.18	31.85	32.35	34.69	27.93	34.04
FeO	0.32	0.36	0.48	0.46	0.48	0.52	0.61	0.68	0.55	0.48	0.54
MgO	n.d.	n.d.	0.03	0.04	0.03	0.05	0.03	0.05	0.03	n.d.	0.03
CaO	8.06	8.81	10.32	10.18	9.58	13.02	15.05	14.75	17.20	9.30	15.89
Na$_2$O	6.51	6.03	4.99	5.22	5.40	3.93	2.95	2.98	1.36	5.73	2.17
K$_2$O	0.31	0.23	0.22	0.21	0.24	0.14	0.08	0.06	0.04	0.20	0.06
Total	99.31	98.22	99.90	100.48	99.66	99.32	99.31	99.72	98.84	98.28	100.22
					Cations based on eight O atoms						
Si	2.591	2.533	2.468	2.480	2.520	2.356	2.248	2.241	2.096	2.500	2.171
Ti	0.001	0.001	0.001	0.001	0.001	0.001	0.000	0.000	0.001	0.001	0.001
Al	1.413	1.471	1.547	1.531	1.488	1.630	1.733	1.751	1.907	1.508	1.836
Fe	0.012	0.014	0.018	0.017	0.018	0.020	0.024	0.026	0.021	0.018	0.021
Mg	—	—	0.002	0.003	0.002	0.003	0.002	0.003	0.002	—	0.002
Ca	0.390	0.434	0.499	0.489	0.463	0.639	0.744	0.726	0.589	0.456	0.779
Na	0.569	0.538	0.436	0.453	0.472	0.349	0.264	0.265	0.123	0.509	0.193
K	0.018	0.013	0.013	0.012	0.014	0.008	0.005	0.004	0.003	0.012	0.004
An	40	44	53	51	49	64	73	73	87	47	80

Note: (1) FT-1, rim; (2) FT-1, adjacent to altered core region; (3) F1, relict rim; (4) F1, adjacent to altered rim; (5) F1, unaltered core; (6) F3, unaltered rim; (7) F3, zone of incipient alteration; (8) F3, adjacent to altered core region; (9) P8-7, unaltered, intermediate between rim and core; (10) P2, rim; (11) P2, core. The abbreviation n.d. = not detected.

ple show significant corrosion around their rims and along fractures. Larger pyroxenes appear to show no visible sign of alteration, except for a fine cloudiness along cleavage planes. Both clasts and groundmass are totally devitrified, and most textures are very hard to distinguish. Fibrous cristobalite is common, as is iron oxide staining throughout.

Sample 212J was taken from along the margin of the vent fissure, and within this sample all phenocrysts and pumice exhibit pervasive replacement. Feldspar phenocryst cores are completely replaced with few exceptions, leaving only relict islands of plagioclase surrounding a dark, porous silica. The surviving plagioclase typically has an atoll structure, and in many cases euhedral feldspar is completely pseudomorphed by silica. Figure 4A is an example of a large feldspar crystal that is partially replaced. Plagioclase in the relict rim ranges from An_{40} at the outer edge to An_{44} adjacent to the altered interior (Table 1, analyses 1 and 2); no remaining feldspars $> An_{45}$ are observed. More severe alteration of larger pyroxenes is also quite evident in this sample (Fig. 4B). Hypersthene ($\approx Wo_3En_{67}$) exhibits corrosion along fractures and especially parallel to (100). Augite ($\approx Wo_{43}En_{18}$) tends to corrode along the outer rim and along fractures throughout the crystals. Likewise, small pyroxene phenocrysts are partially or completely replaced from the exterior by the same processes. Textures in the pumice are nearly completely destroyed, as much of the sample has been replaced by cristobalite. Original clasts are recognizable only by outlines of iron oxide.

TEM OBSERVATIONS

Plagioclase textures

A number of plagioclase phenocrysts from samples 212L and 212J and one augite phenocryst from 212J were selected for transmission electron microscope studies. TEM observation of partially altered phenocrysts from both samples has revealed complex reaction microstructures present in the replacement zones and provides some insights into the mechanisms of the alteration reactions.

Sample 212L. As noted above, plagioclase in sample 212L shows evidence of incipient local alteration along growth zones. TEM observations indicate that two distinct zones are present within the regions of alteration, which can be discriminated on the basis of their microstructural and compositional characteristics. Typically, the zones occur in a layered arrangement from unaltered plagioclase into the altered region. The innermost zone, immediately adjacent to the feldspar interface, consists of a layer of an amorphous Al-bearing, silica-rich phase and varies in width from <1 to over 3 μm. A second layer, consisting entirely of amorphous silica, makes up the central portion of the alteration zone.

The interface between the plagioclase and silica-rich inner layer is invariably sharp and well defined. Compositionally this inner zone consists of $\sim$85 wt% SiO_2, 8 wt% Al_2O_3 with 1–2 wt% CaO, Na_2O, and K_2O, as well
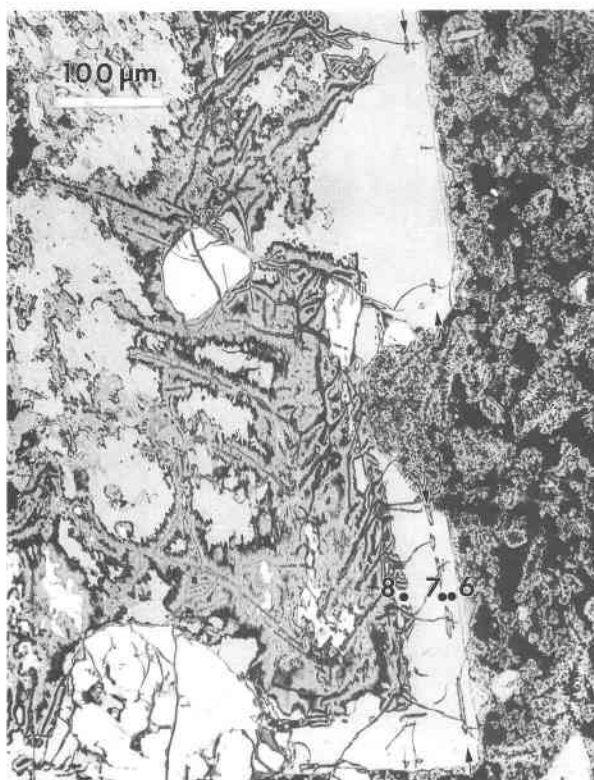

Fig. 2. BSE image of a partially altered plagioclase (light gray) from 212L, in which the calcic core has been replaced by amorphous SiO_2 (dark gray). Oscillatory zoning is present in this feldspar, which ranges from An_{64} at the rim to An_{70} at the edge of the altered core. Incipient alteration can be observed along a calcic zone (arrows) of An_{70}–An_{73} that has been partially replaced within the relict plagioclase. Numbers correspond to analyses in Table 1.

as minor concentrations of Cl. Analytical electron microscope analyses (AEM) of the amorphous phase (normalized to 100 wt%) are reported in Table 2. Detailed AEM analyses across the interface between plagioclase and amorphous silica show that there is a remarkable increase in Cl concentrations immediately adjacent to the plagioclase. This increase occurs in a zone about 1000 Å in thickness, in which Cl may reach concentrations as high as 12.5 wt% and Ca is depleted, along with Al, relative to stoichiometric feldspar.

The inner zone of impure amorphous silica locally contains patches or clusters of very fine-grained phyllosilicates, which have a wavy, curved morphology. Individual clusters may be up to 1.5 μm in size, but isolated crystallites only a few tens of ångströms in length can also occur. AEM analyses of clusters of phyllosilicates show that they are aluminous in character, with variable Si/Al ratios between 1.2 and 1.8 and FeO contents of 3.5–4.8 wt%. CaO is also present in concentrations <3 wt%. This phase is relatively unstable in the electron beam and is damaged by the beam rapidly. However, it was possible to obtain high-resolution TEM images using low-dose
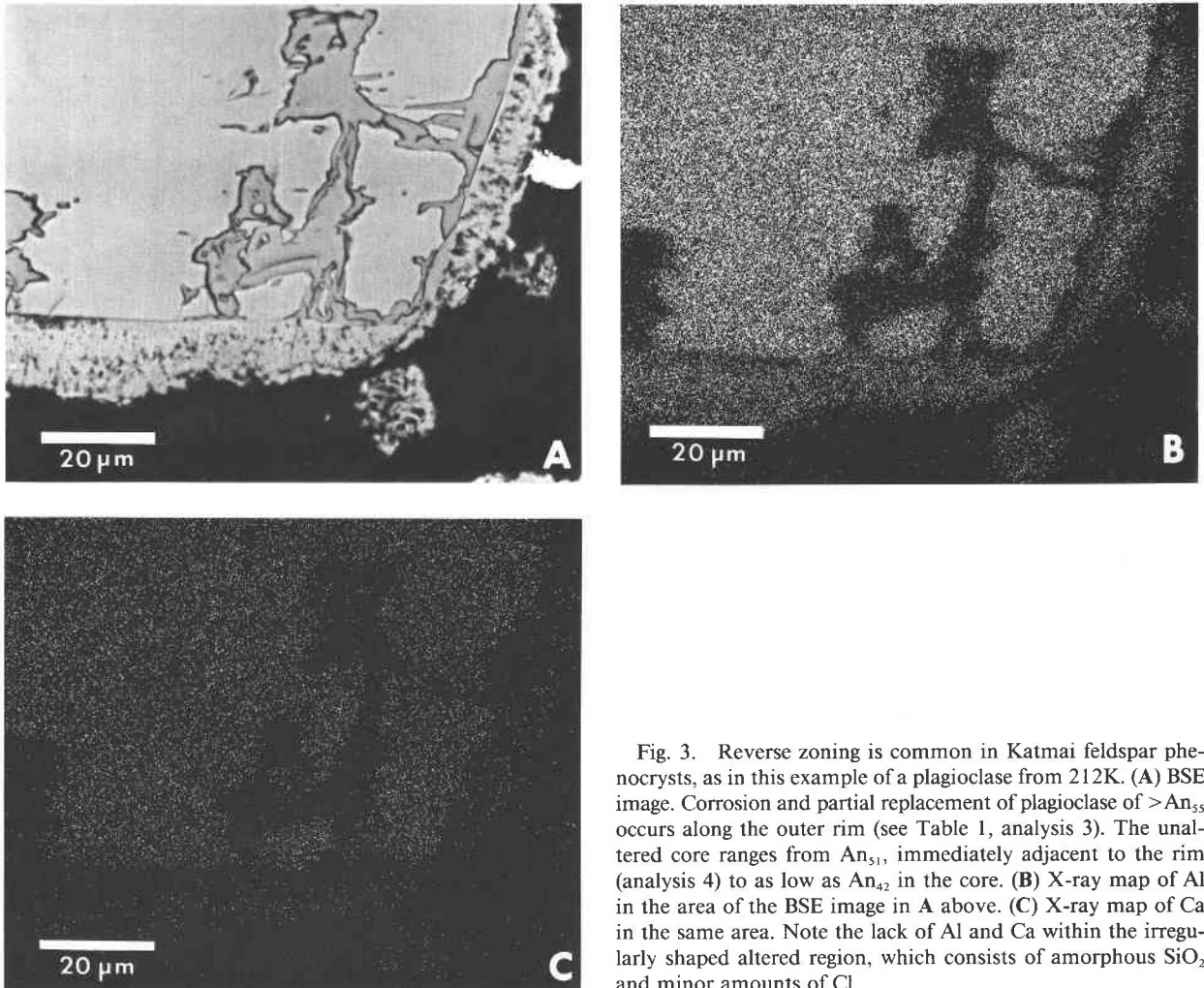
Fig. 3. Reverse zoning is common in Katmai feldspar phenocrysts, as in this example of a plagioclase from 212K. (A) BSE image. Corrosion and partial replacement of plagioclase of $>An_{55}$ occurs along the outer rim (see Table 1, analysis 3). The unaltered core ranges from An_{51}, immediately adjacent to the rim (analysis 4) to as low as An_{42} in the core. (B) X-ray map of Al in the area of the BSE image in A above. (C) X-ray map of Ca in the same area. Note the lack of Al and Ca within the irregularly shaped altered region, which consists of amorphous SiO_2 and minor amounts of Cl.

techniques, which show basal lattice fringes between 10 and 12 Å (Fig. 5A). There are problems with interpreting one-dimensional lattice-fringe images for phyllosilicate minerals, which have been discussed in detail by Guthrie and Veblen (1990). However, we have only measured d values from images recorded at the appropriate focus conditions, as suggested by Guthrie and Veblen (1990), so that the measured lattice spacings should be diagnostic of the phyllosilicate phase present. The Si/Al ratios for the analyzed phyllosilicate clusters appear to be most consistent with Al-rich smectite, such as beidellite. Ideal end-member beidellite has an Si/Al ratio of 1.25 (Newman and Brown, 1987) but varies depending on the degree of Al substitution. Ca can also be accommodated into beidellite as the interlayer cation, accounting for the presence of Ca in the analyses. The observed variation in the measured lattice spacings is also compatible with beidellite because smectite collapses to varying degrees in the high vacuum of a TEM (Ahn and Peacor, 1986; Klimentidis and Mackinnon, 1986).

The central part of the reaction zone consists entirely of amorphous silica with a distinct mottled diffraction contrast (Fig. 5B), which is separated from the inner layer by a sharp interface. This amorphous silica is compositionally distinct from the amorphous silica-rich phase in the inner zone in having lower concentrations of Al_2O_3 (<1.2 wt%) and alkalis that are close to detection limits for energy-dispersive analysis.

Sample 212J. Most plagioclase crystals in this sample are extensively replaced by silica, but one was found that exhibited evidence of only partial replacement in its core region. Optically this phenocryst exhibits a wormlike replacement texture, which is restricted to the more calcic central zone of the crystal (Fig. 6). Fractures are present from the core to the rim, which provided pathways for infiltrating fluids. TEM images show that replacement of the feldspar occurs by the formation of kite-shaped (in cross section) regions distributed throughout the core region (Fig. 7A, 7B), which are filled with amorphous silica and other phases (see below). These altered zones, which
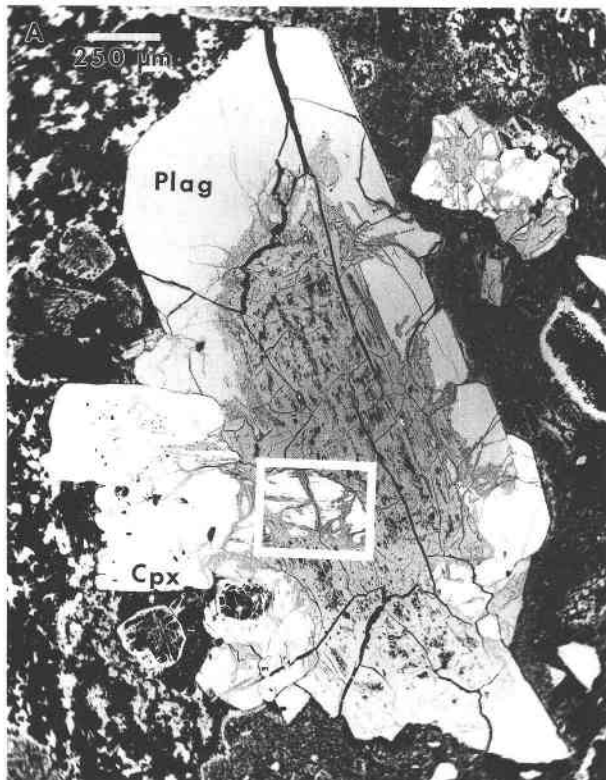
Fig. 4. BSE images of plagioclase and pyroxene from sample 212J. (A) The wide rim is all that remains of this normally zoned plagioclase (Plag), in which the more calcic compositions ($>An_{44}$) that probably existed in the central portion have been replaced. Both augite (Cpx) and hypersthene (in box) are present as inclusions in the feldspar, and both exhibit varying degrees of alteration, particularly along cleavages and fractures. (B) Enlarged view of hypersthene within the box in A. Initial alteration along (100) cleavage planes and in fractures is evident.

vary in size from 0.5 to 5 μm, are probably tubular in three dimensions and extend through the feldspar for several hundred micrometers. Individual, isolated, tubular replacement zones appear to develop randomly within the crystal but coalesce as they grow (Fig. 7A). At intermediate stages in this alteration process, islands of relict feldspar may still persist, surrounded by amorphous silica. Individual alteration zones all exhibit a distinct concentric zonal or layered sequence, which is dominated by a central region of amorphous silica, surrounded by a narrow rim immediately adjacent to the altering plagioclase (Fig. 7A, 7B). This narrow rim has a variable thickness from 5000 to <200 Å and typically appears lighter than the core of amorphous silica in TEM images. These differences in contrast are probably caused by variations in thickness, produced during ion milling. In some cases, two generations of this type of zonal sequence are present, with a small central core concentrically enclosed within a larger alteration sequence (Fig. 7B).

The interface between plagioclase and replacement phases is typically slightly curved, although some interfaces may be highly planar, such as that along (1$\bar{1}$0) in Figure 7A. There is some evidence for crystallographic control on the rate of the reaction, as indicated by the thickness of the narrow zones between the central region of amorphous silica and unaltered plagioclase. This zone is typically significantly thicker parallel to (1$\bar{1}$0) than to (10$\bar{2}$).

Detailed TEM studies of the narrow layer adjacent to

plagioclase show that this zone actually consists of two compositionally distinct layers, both consisting of amorphous material (Fig. 7C). The layer immediately adjacent to plagioclase is extremely thin (<500 Å) and appears slightly darker in TEM images than the second layer (Fig. 7C). This second layer has an extremely sharp interface with the central region of amorphous silica. Compositionally, the inner layer immediately adjacent to plagioclase is depleted in SiO_2 relative to plagioclase but is extremely enriched in Cl and S. With data normalized to 100 wt%, Cl and S concentrations can reach as high as

TABLE 2. Analytical electron microscope analyses of plagioclase and alteration phases from samples 212L and 212J

	1 212L	2 212L	3 212L	4 212L	5 212J	6 212J	7 212J	8 212J
SiO_2	85.0	95.4	53.0	54.3	59.0	56.3	82.9	97.9
TiO_2	0.80	n.d.	n.d.	n.d.	n.a.	n.a.	n.a.	n.a.
Al_2O_3	7.0	1.3	36.9	37.7	25.4	18.4	13.4	1.7
FeO	n.d.	n.d.	4.9	5.0	n.a.	n.a.	n.a.	n.a.
MgO	n.d.	n.d.	n.d.	n.d.	n.a.	n.a.	n.a.	n.a.
CaO	3.0	1.1	2.8	1.9	9.1	0.1	2.5	0.2
Na_2O	1.5	0.1	0.1	n.d.	6.2	0.3	0.8	n.d.
K_2O	1.1	1.4	0.8	n.d.	0.2	0.1	0.3	0.1
Cl	1.6	0.7	1.5	1.1	n.d.	22.0	0.1	0.1
S	n.d.	n.d.	n.d.	n.d.	0.1	2.9	n.d.	n.d.

Note: (1) leached surface area on plagioclase; (2) amorphous silica; (3) and (4) halloysite; (5) plagioclase; (6) leached surface layer; (7) amorphous aluminosilicate; (8) amorphous silicate. The abbreviations n.a. and n.d. = not analyzed and not detected, respectively. Analyses normalized to 100 wt%.
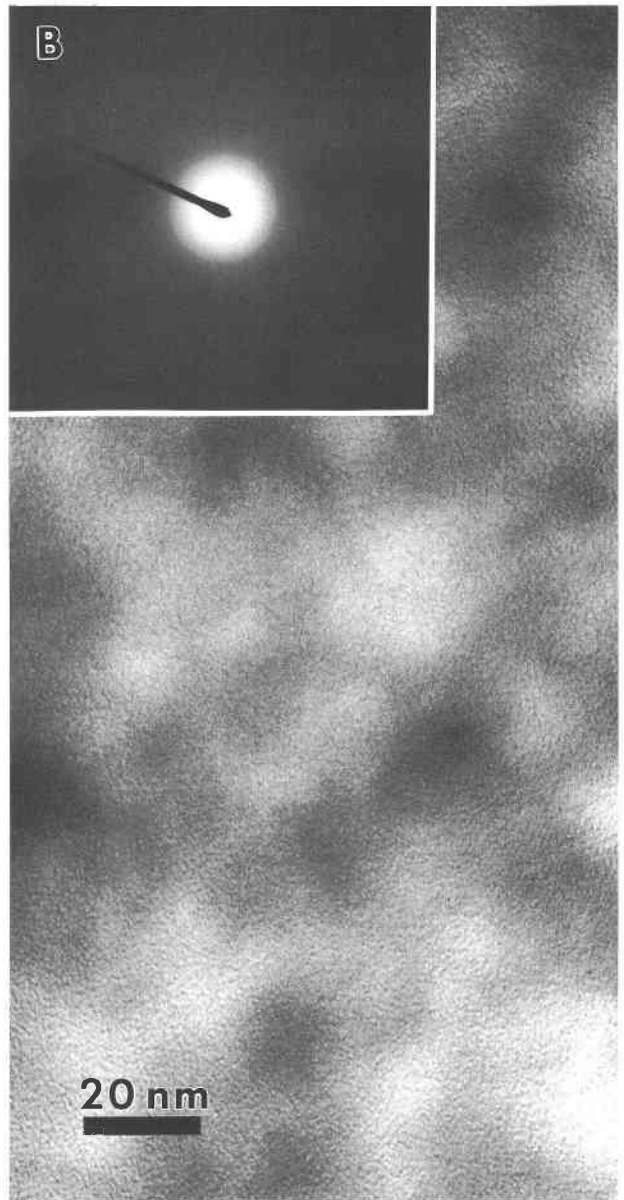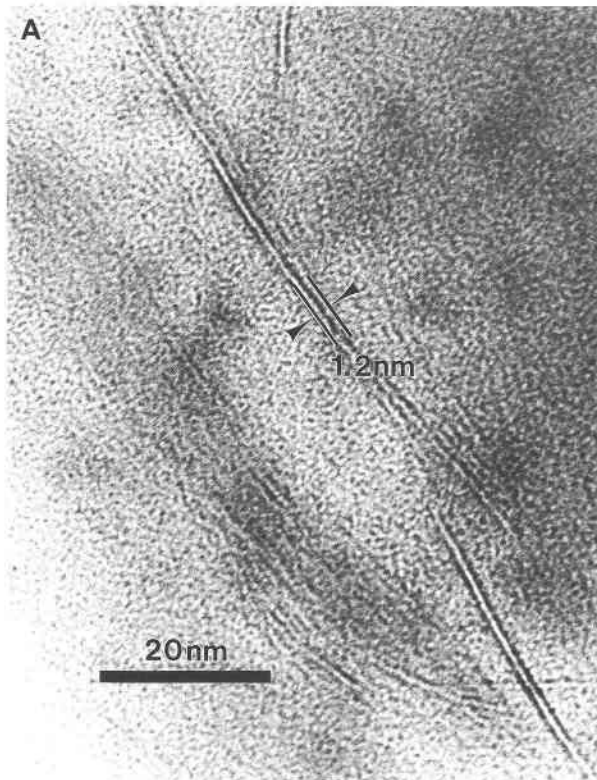
Fig. 5. Transmission electron micrographs showing examples of textures within the replacement zones. (A) Microcrystallites of Al-rich smectite with an apparent basal spacing of 10–12 Å set in an amorphous silica matrix. (B) Fine microstructure observed in the central zone of amorphous silica. The amorphous material exhibits an unusual mottled contrast and appears to consist of distinct domains, which appear dark and light in the image. No lattice fringes can be resolved, but that may indicate that local ordering or compositional variations only occur on a very fine scale.

20 and 16 wt%, respectively. Cl concentrations are, however, typically much higher than those of S. CaO, Na_2O, and Al_2O_3 are only slightly depleted relative to stoichiometric feldspar. In comparison the second layer shows only modest enrichment in Cl and S, and SiO_2 is not depleted. The final, dominant central region of the replacement zone is essentially pure silica, with some minor Al_2O_3 (<2 wt%). The compositional variations across the layered sequence are summarized in Figure 8 and Table 2.

The interface region between the amorphous SiO_2 and unreacted rims in highly altered feldspar phenocrysts, e.g., Figure 9A, was also studied by TEM. Optically, the interface region consists of a cloudy zone in which dark vermicular veins intrude into the feldspar for several mi-

crometers (Fig. 9B). In TEM images, the interface zone exhibits many of the complexities observed in the less altered phenocrysts. Several distinct zones of amorphous phases have formed, replacing the feldspar. These are illustrated in Figure 9C, which shows a roughly square region of amorphous material, consisting of a central dark core with mottled contrast, surrounded by a zone of material with lighter contrast. In detail, the central zone contains several narrow concentric rings. The core region is impure amorphous silica with about 2–3 wt% Al_2O_3, but the rim is compositionally complex and is enriched in Al_2O_3, FeO, and S up to 3 wt%. Microstructures of this type, consisting of several distinct zones of amorphous material, occur throughout regions of replaced feldspar, not just close to the interface. They frequently form com-

TABLE 3. Analytical electron microscope analyses of augite and alteration phases from sample 212J

	1	2	3	4
SiO$_2$	53.1	72.6	68.1	97.1
TiO$_2$	0.9	0.9	0.6	n.d.
Al$_2$O$_3$	4.8	2.4	27.2	0.3
FeO	11.6	20.0	2.8	1.0
MgO	10.3	2.2	1.1	0.8
CaO	19.2	1.2	0.2	0.1
Na$_2$O	0.1	n.d.	n.d.	0.7
K$_2$O	n.d.	0.7	n.d.	n.d.

Note: (1) augite; (2) leached surface zone; (3) halloysite; (4) amorphous silica. The abbreviation n.d. = not detected. Analyses normalized to 100 wt%.

plex textural relationships that appear to be the result of the growth and coalescence of several alteration zones, such as those found in the less altered plagioclase. This type of microstructure clearly gives rise to the complex textures commonly observed optically in pseudomorphed phenocrysts.

Augite textures

Backscattered electron imaging of sample 212J shows that augite has been preferentially replaced along fractures and along cleavage planes indicating, in the latter case, a crystallographic control on the replacement reaction (Fig. 4B). TEM studies of replacement zones along cleavage planes show that a zoned reaction sequence of phases is present, similar to that found in altering feldspar. There are, however, a number of important differences. Figure 10A illustrates a small elongate replacement zone that has developed with planar interfaces parallel to (100) augite. The zoned characteristics of the alteration are apparent, with three distinct layers arranged symmetrically from the center of the replaced region. These are (1) a narrow layer (200–300 Å) immediately adjacent to augite, which shows light contrast in TEM images, (2) a narrow diffuse porous zone that grades into (3) a thick, dark central region with dark contrast. Like the replacement zone in plagioclase, this central region has been shown by AEM and electron diffraction techniques to be almost pure amorphous silica. The diffuse porous layer has a complex microstructure and contains a phase that clearly has a cylindrical morphology, with cylinder diameters of 500–700 Å (Fig. 10B). This phase is extremely beam sensitive and damages very rapidly. AEM studies show that regions of this phase contain only SiO$_2$ and Al$_2$O$_3$, with minor FeO. The cylindrical morphology of this phase is most consistent with halloysite (e.g., Tazaki, 1982), but the Si/Al ratio is too high (2.1–2.5, as opposed to 1). This does not necessarily preclude halloysite but probably indicates that significant amorphous silica is present as a matrix that is intimately intergrown with the halloysite and, consequently, is present in any analysis area. The layer of halloysite grades rapidly into the inner layer adjacent to augite. Compositionally this inner layer is enriched in SiO$_2$ and FeO relative to augite but is com-
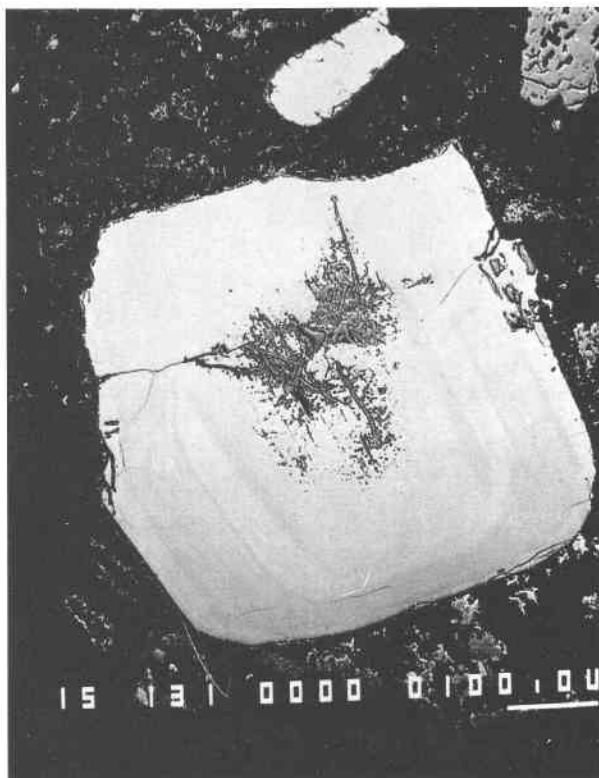

Fig. 6. BSE image of a partially altered plagioclase phenocryst from sample 212J. Scale bar is 100 μm. The core of the plagioclase has been extensively altered, and replacement has taken place by the development of a vermicular texture, with abundant narrow tubes. Locally, where cracks extend to the rim, alteration is more extensive, indicating that the cracks acted as pathways for infiltrating fluids.

pletely free of MgO and CaO (Fig. 11). Unlike the innermost amorphous layer produced in plagioclase alteration, there is no evidence of any S or Cl. Representative AEM analyses of these zones are reported in Table 3.

Significantly more alteration has occurred along fractures in augite. These zones have extremely irregular interfaces with augite and exhibit complex microstructures (Fig. 12A). Rather than a simple layered sequence of alteration phases, the fractures are dominated by pure amorphous silica, which contains narrow bands (<0.2 μm) of amorphous porous material that lie parallel to the sides of the fractures. These bands extend for several tens of micrometers along individual fractures (Fig. 12B) and contain Al$_2$O$_3$ and FeO in addition to SiO$_2$, although the concentrations of these elements are generally low. Locally, the bands consist of sets of small veins <200 Å in thickness, which may be continuous but pinch out within the amorphous silica.

CHEMICAL MASS TRANSPORT

Figure 13A portrays the modal abundance of the major crystalline minerals in samples J–O as determined by
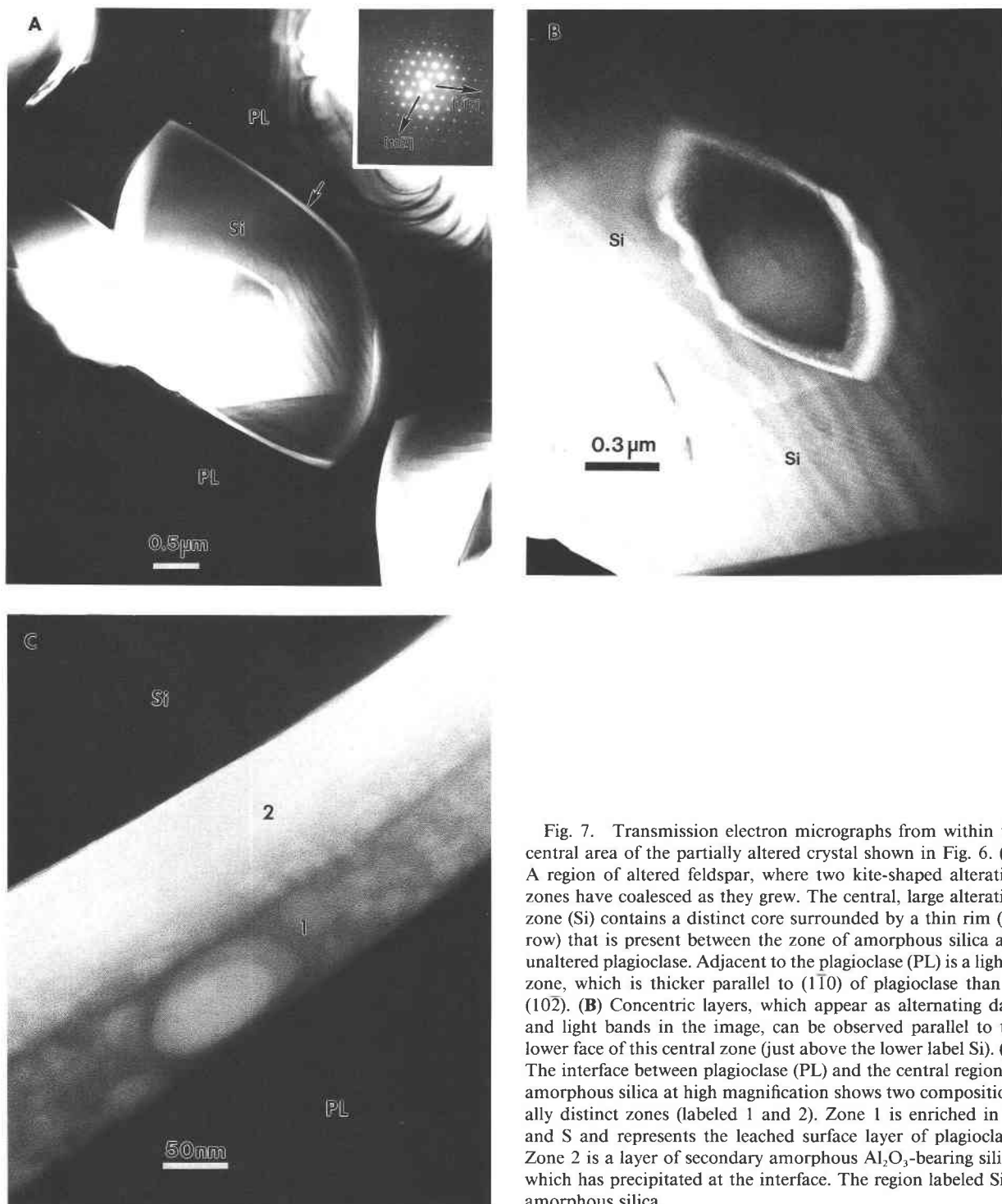
Fig. 7. Transmission electron micrographs from within the central area of the partially altered crystal shown in Fig. 6. (A) A region of altered feldspar, where two kite-shaped alteration zones have coalesced as they grew. The central, large alteration zone (Si) contains a distinct core surrounded by a thin rim (arrow) that is present between the zone of amorphous silica and unaltered plagioclase. Adjacent to the plagioclase (PL) is a lighter zone, which is thicker parallel to $(1\bar{1}0)$ of plagioclase than to $(10\bar{2})$. (B) Concentric layers, which appear as alternating dark and light bands in the image, can be observed parallel to the lower face of this central zone (just above the lower label Si). (C) The interface between plagioclase (PL) and the central region of amorphous silica at high magnification shows two compositionally distinct zones (labeled 1 and 2). Zone 1 is enriched in Cl and S and represents the leached surface layer of plagioclase. Zone 2 is a layer of secondary amorphous Al_2O_3-bearing silica, which has precipitated at the interface. The region labeled Si is amorphous silica.

quantitative X-ray diffraction by Papike et al. (1991b). The depletion of plagioclase and pyroxene can be clearly seen as the fumarole conduit is approached. Likewise, an enrichment of α cristobalite adjacent to the vent is apparent and has been noted in many of the fumaroles at Katmai (Keith, 1985, 1991a, 1991b). For the most part,

the modal abundance of the major minerals follows that observed in the optical descriptions presented above. However, the XRD modes indicate that the proportion of pyroxene systematically diminishes toward the vent, whereas optical examination does not indicate a significant amount of pyroxene phenocryst alteration outside of

the two samples closest to the vent. Apparently, substantial numbers of small phenocrysts are being altered, which would account for the loss of pyroxene farther from the conduit. In addition, the volume of alunite that is indicated in the XRD modes was largely underestimated in the optical studies.

In a previous study of these samples, Papike et al. (1991b) used a mathematical line-fitting function to estimate the chemical gains and losses resulting from fumarolic alteration. The slopes of best-fit isocons (Grant, 1986) can be used to assess changes in rock mass that occur during alteration. This approach allows us to quantify the chemical transport in this dynamic system, including both the influx of Si and other elements from the hot fumarolic gases and hydrothermal fluids and the leaching of Al, Na, and Ca from the dacitic tuff adjacent to the fumarole vent (Fig. 13B). Strong enrichment of silica is observed in the four samples closest to the vent, and only minor enrichment farther from the vent. A concomitant enrichment in cristobalite is observed in the modal proportions, at least in the two samples nearest the vent (Fig. 13A), although four samples near the vent have a high amorphous silica content (Papike et al., 1991b). The enrichment of Si in these samples can be attributed to the presence of both cristobalite and opal close to the vent (Keith, 1991a). The enrichment of Si is an indication that the plagioclase and other minerals in the tuff not only underwent leaching processes, whereby Al, Ca, and Na were removed from the mineral structure leaving residual Si, but also experienced an influx of additional Si that was incorporated into the pseudomorphs.

All the elements plotted in Figure 13B show some degree of depletion immediately adjacent to the vent, as a result of leaching by the hot fumarolic gases and hydrothermal fluids. In sample J, Al shows strong depletion but rebounds in samples L and M to a slight enrichment before reaching zero-mass change in the two outer samples. The depletion of Al in samples J and K coincides with a decline in the modal abundance of plagioclase in the vicinity of the vent, whereas the slight enrichment of Al corresponds to the presence of alunite in samples K, L, and M (Fig. 13A).

DISCUSSION

Fumarolic activity at Katmai has undergone a complex evolution, which has been documented in detail by Papike et al. (1991a, 1991b) and Papike (1992). Early stages of fumarole development involved the formation of sublimates as a result of elemental mass transport at high temperatures in the vapor phase. The early vapor phase was a mixture of magmatic gases released by the cooling outflow sheet and meteoric H_2O from streams, snow, and ice that was buried by the pyroclastic flow. As cooling proceeded, fumarole vapor condensed and mixed with fresh meteoric H_2O. These fluids interacted extensively with the protolith material adjacent to the fumarole vent, causing alteration of early-formed fumarolic minerals, as well as primary magmatic phases and glasses. It is during
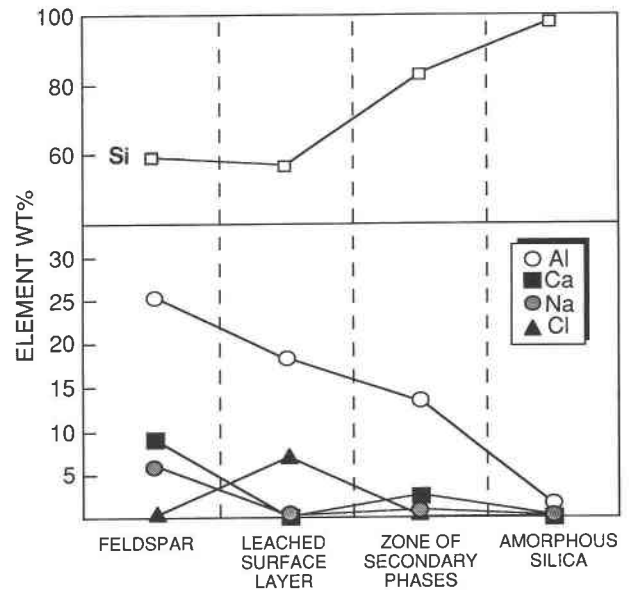

Fig. 8. Normalized element concentrations are plotted, illustrating the compositional variations that occur in a traverse from plagioclase into the leached surface layer and through subsequent layers of amorphous Al-bearing silica and pure silica (AEM data).

this later period of fumarole activity that alteration of plagioclase and pyroxene appears to have occurred. The presence of halloysite and smectite indicate that alteration, at least in its later stages, occurred at temperatures below ~200 °C, since halloysite transforms to kaolinite above 110 °C (Hurst and Kunkle, 1985), and smectite begins to transform to illite between 100 and 150 °C (e.g., Velde and Meunier, 1987). In the early stages of alteration, however, temperatures must have been higher, probably in the range 200–350 °C, since fumarole gas temperatures over 400 °C were documented by Allen and Zies (1923) and Zies (1929).

Based on the chemistry of fumarolic gases at Katmai, it is clear that the altering fluids were extremely acidic. Gas compositions of 0.117 vol% HCl, 0.032 vol% HF, and 0.029 vol% H_2S were recorded by Allen and Zies (1923) and Zies (1929) while the fumaroles were still active. Analysis of condensates at St. Augustine volcano, near Katmai in the Aleutian Range, yielded Cl concentrations of 6600–47000 ppm for rooted fumaroles and 7800–28000 ppm for pyroclastic flow fumaroles (Symonds et al., 1987). Similarly, F concentrations of 480–5400 and 50–1100 ppm, respectively, were recorded, and values for pH measured in the field were <0.5.

Kodosky and Keskinen (1990) pointed out that reactions involving liquid phases resulting from the condensation of acid vapors appear to be the dominant mechanism of alteration in volcanic systems. This conclusion is based on the high structural and nonstructural H_2O content of altered minerals, relative to unaltered ash, as well as the morphology of the encrusting phases. Indeed, the primary source of fumarolic encrustation components
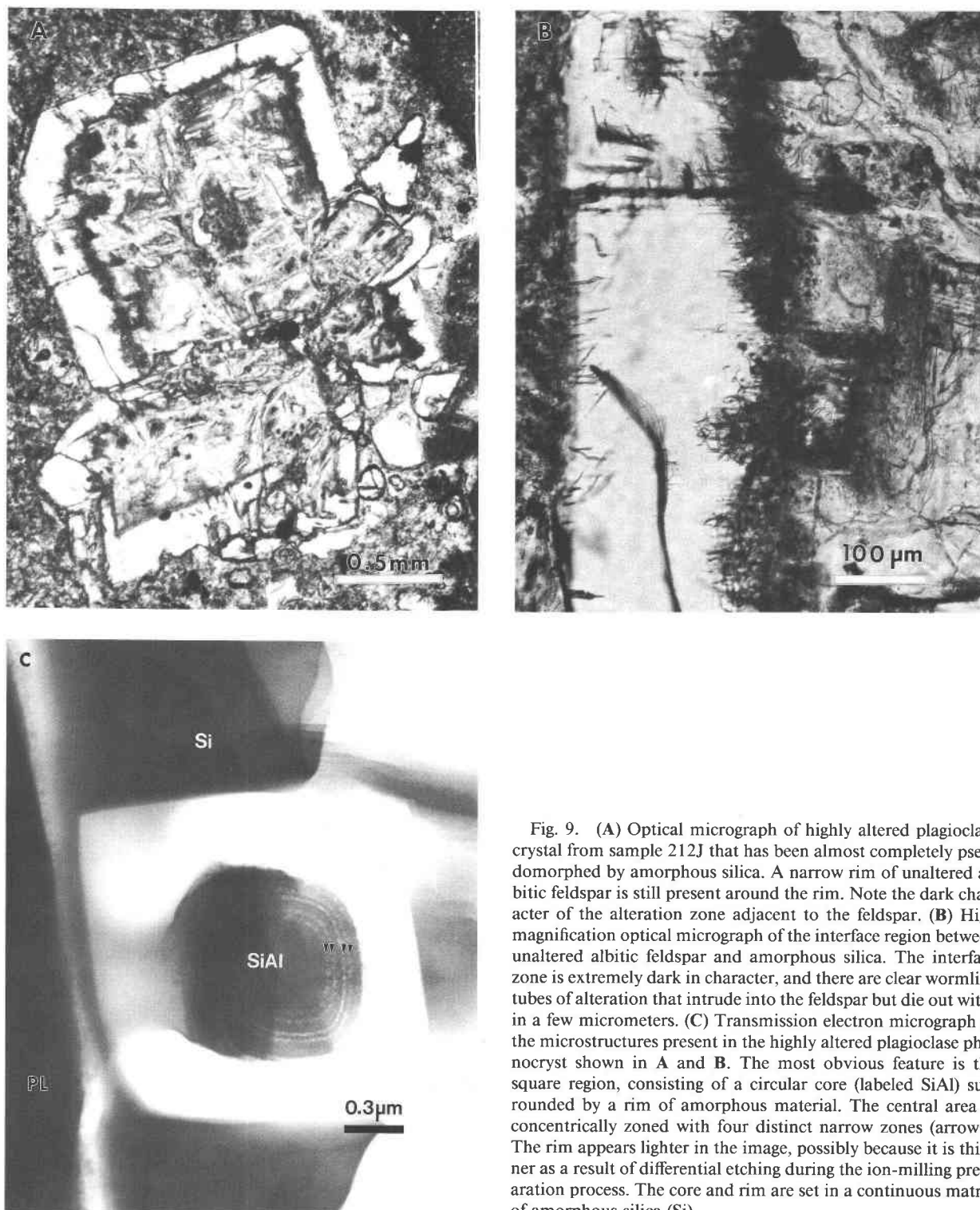
Fig. 9. (A) Optical micrograph of highly altered plagioclase crystal from sample 212J that has been almost completely pseudomorphed by amorphous silica. A narrow rim of unaltered albitic feldspar is still present around the rim. Note the dark character of the alteration zone adjacent to the feldspar. (B) High magnification optical micrograph of the interface region between unaltered albitic feldspar and amorphous silica. The interface zone is extremely dark in character, and there are clear wormlike tubes of alteration that intrude into the feldspar but die out within a few micrometers. (C) Transmission electron micrograph of the microstructures present in the highly altered plagioclase phenocryst shown in A and B. The most obvious feature is the square region, consisting of a circular core (labeled SiAl) surrounded by a rim of amorphous material. The central area is concentrically zoned with four distinct narrow zones (arrows). The rim appears lighter in the image, possibly because it is thinner as a result of differential etching during the ion-milling preparation process. The core and rim are set in a continuous matrix of amorphous silica (Si).

at Katmai is the leaching of tephra by these condensed acid vapors (Keith, 1991b).

Alteration of plagioclase

The interaction of feldspars with aqueous fluids has been studied extensively in the laboratory (e.g., Holdren

and Berner, 1979; Chou and Wollast, 1985; Casey et al., 1989; Hellmann et al., 1990) and in a number of geological systems, particularly those involving weathering phenomena and hydrothermal alteration at low temperatures (e.g., Eggleton and Buseck, 1980; Banfield and Eggleton, 1990). These studies show that the dissolution rate and
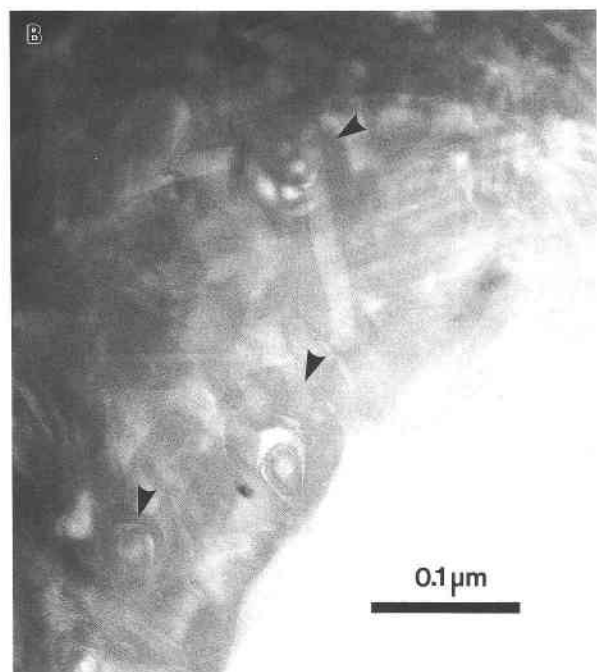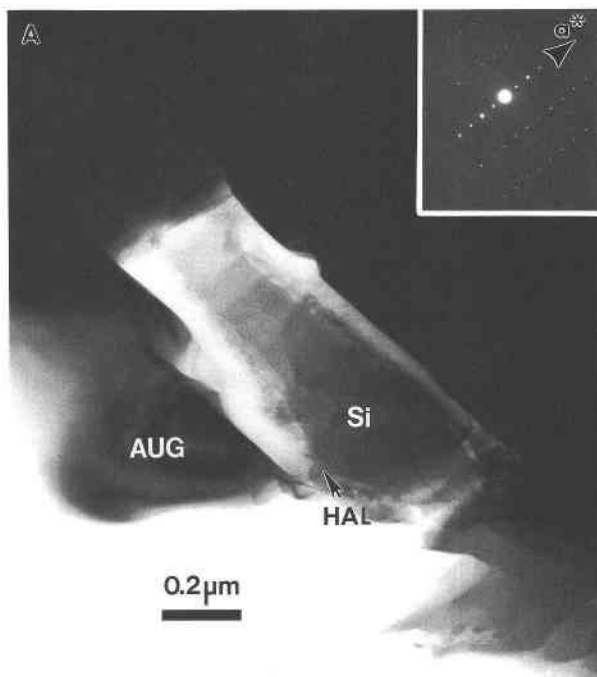
Fig. 10. (A) Transmission electron micrograph of a narrow zone of alteration parallel to (100) in an augite phenocryst from sample 212J. A layer of microcrystalline halloysite (HAL) separates the central zone of amorphous silica from a leached layer of pyroxene that is depleted in Ca and Mg. (B) High-magnification TEM image showing the microstructural characteristics of halloysite in the alteration zone. The typical cylindrical or tubular morphology is apparent in many crystals, some examples of which are marked with arrows.
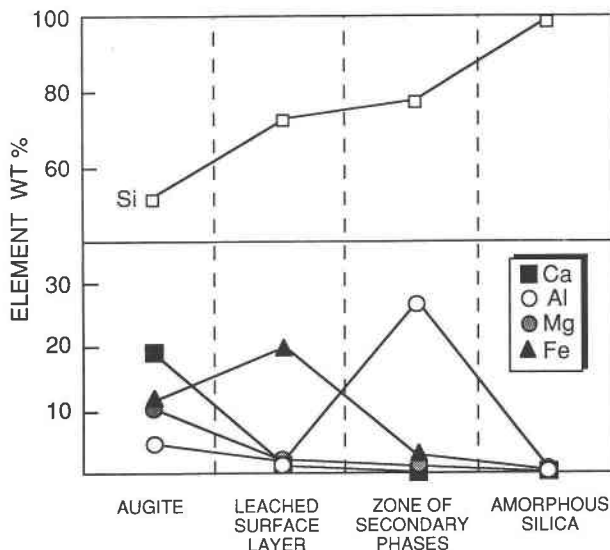

Fig. 11. Diagram showing normalized AEM analyses on a traverse from unaltered augite into the alteration zone, which consists of three distinct layers. The leached layer immediately adjacent to augite is depleted in Ca and Mg. The second layer consists of secondary phases that have precipitated from the fluid phase, and the outer zone is a region of amorphous silica.

reaction products are functions of the composition of the feldspar, temperature, pH, and the chemistry of the aqueous fluid. Such studies provide a framework for examining the alteration mechanism of feldspar in an extreme geochemical environment such as occurs in the fumarole systems at Katmai.

The high Cl and low pH of the fumarolic fluids has had a profound effect on the alteration of plagioclase observed in this suite of samples. In our study, the breakdown of feldspar phenocrysts begins with the most calcic plagioclase ($>An_{87}$) in sample 212N at some distance from the conduit. At 10 cm from the conduit, incipient alteration occurs at $>An_{73}$, but at 5 cm, only plagioclase $<An_{51}$ survives. Immediately adjacent to the vent, no compositions above An_{45} are observed. Greater An values are inferred to have been present in the rims or cores of these now-altered phenocrysts, since high An values are observed in the cores and rims of plagioclase phenocrysts in the unaltered tuff. The lack of occurrence of progressively lower An compositions as the vent is approached is the result of dissolution of these compositions during alteration. This observation agrees with the measurements by Casey et al. (1991), who noted that dissolution rates of plagioclase in acid solutions are sensitive to mineral composition. This progressive destruction of more sodic plagioclase, as the fumarole is approached, can be explained by the solution equilibria of plagioclase in chloride-bearing solutions. Helgeson (1974) has shown that calcic plagioclase is significantly more soluble in chloride-rich solutions than albite at low temperatures, such that destruction of anorthitic plagioclase will occur preferentially to albite. However, with increasing temperature, the
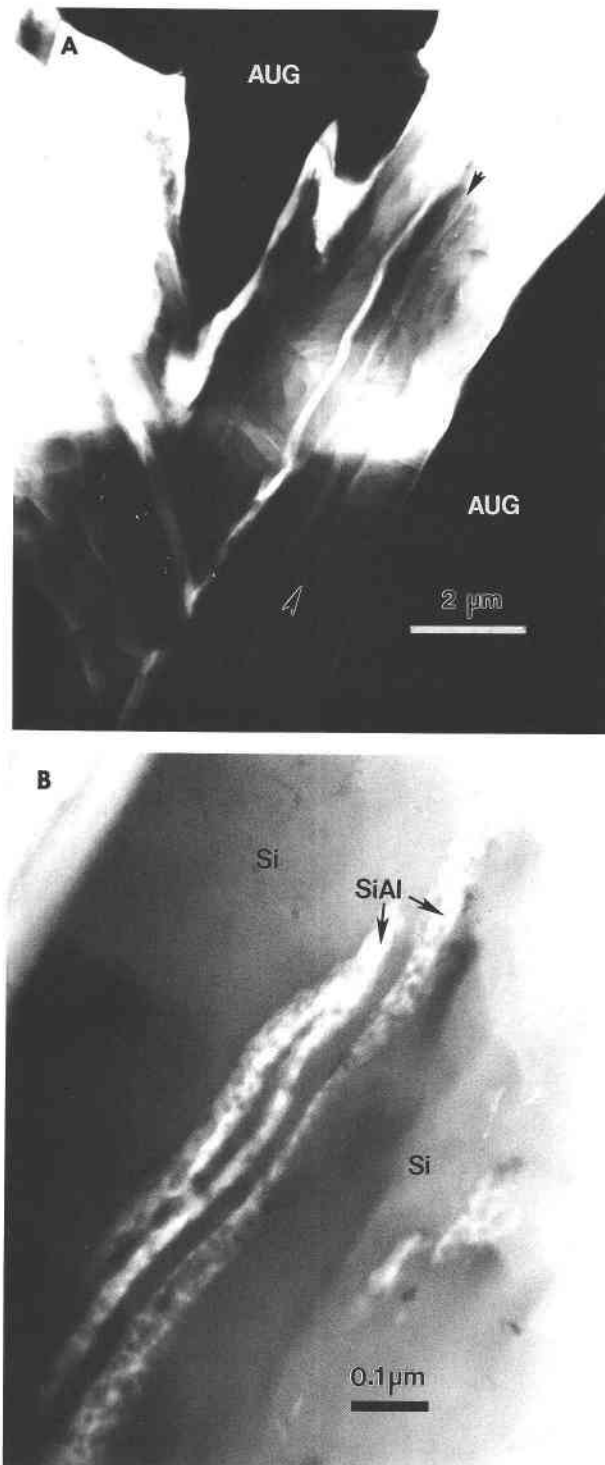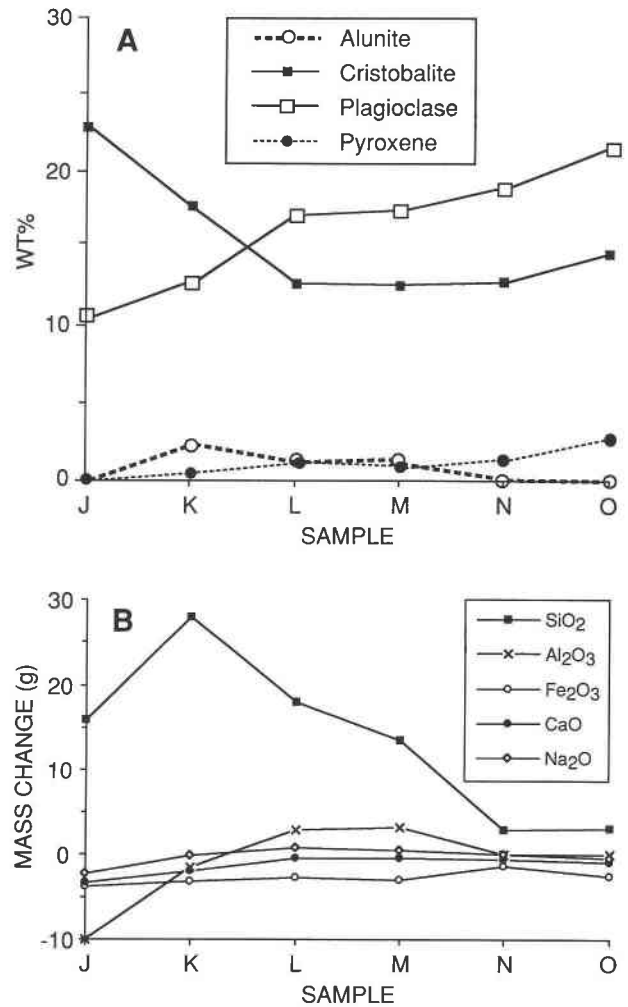
Fig. 13. (A) Modal proportions of the crystalline phases from the conduit (at sample J) outward to unaltered tuff (sample O). Note the depletion of plagioclase and pyroxene adjacent to the conduit and the enrichment of cristobalite and alunite. From Papike et al. (1991b). (B) The gains and losses of major elements outward from the conduit. The vertical scale corresponds to the grams of each element gained or lost during alteration relative to 100 g of unaltered dacite, as determined by the isocon method (Grant, 1986).

Fig. 12. (A) Low-magnification transmission electron micrograph of alteration along a large fracture in augite. The alteration is dominated by amorphous silica, but several narrow bands (arrows) of mottled contrast occur parallel to the edges of the fracture. (B) High-magnification TEM image of thin bands of amorphous Al-bearing silica shown in A. The bands appear to have a high porosity and probably represent channels along which fumarolic fluids infiltrated the interior of the crystal.

solubility of calcic plagioclase decreases significantly, and albite becomes more unstable (Helgeson, 1974). In addition, the rate of albite dissolution at low pH is enhanced by rapid cation exchange (Yang and Kirkpatrick, 1989). Therefore both the low pH and high chlorinity of fumarolic gases, along with the expected increase of temperature closer to the conduit, have resulted in the replacement of more sodic plagioclase closer to the vent.

Electron microprobe analyses of the Katmai samples show that selective extraction of Ca, Na, and Al from plagioclase and replacement by amorphous silica has occurred. Our TEM observations provide evidence for the detailed mechanism of this replacement reaction and show that alteration of plagioclase involves the formation of

several surface layers in the interior of the feldspar. Alteration initially involves the formation of a very thin surface layer that is enriched in Cl and depleted in Ca, Na, and Al relative to stoichiometric feldspar. The formation of a thin leached surface layer is consistent with experimental studies of feldspar dissolution in aqueous solution at high pH (e.g., Chou and Wollast, 1985; Casey et al., 1989; Hellmann et al., 1990). These studies show that the early stages of alteration of plagioclase proceed by incongruent dissolution reactions in a multistep process involving hydrolysis reactions at the mineral-fluid interface and the formation of a leached, silica-rich surface layer. The depth of the surface layer appears to be dependent on the pH conditions under which alteration occurs and may also be affected by temperature. Depth profiles by SIMS analysis (Muir et al., 1989) indicate that for labradorite leached in H_2O only, the zone of Al depletion is 60–120 Å thick, and the zone of Ca depletion is up to 100–200 Å thick, but for samples leached in HCl (pH = 3.5), the layer is 600–1200 Å. The data also indicate the presence of a step in the layer, which may correspond to the formation of a secondary phase layer. These values are consistent with XPS measurements on albite reacted at pH 0.47–2.49 at 225 °C, which had been leached to depths of 600–900 Å (Hellmann et al., 1990). The thickness of the leached layer in these experimental studies is entirely consistent with the layer found in partially altered feldspar in sample 212J, where a 500 Å leached layer has developed.

Hellmann et al. (1990) also reported the presence of Cl in the leached layer, which is present to a depth of 700 Å in albite leached at pH 0.57 at 225 °C. It appears that this solute penetrates the leached surface layer to the same depth as H_2O. The presence of Cl in the leached layer in the Katmai plagioclase may also be attributed to the electrostatic absorption of Cl^- at charged sites within the leached layer (Hellmann et al., 1990). On the basis of the experimental work of Hellmann et al. (1990) it is clear that the presence of Cl in the leached layer is an indicator of low pH in the system, since at 225 °C, Cl absorption was only found to occur at pH < ~2.26.

Provided the altering fluids remain undersaturated relative to the solubilities of phases such as kaolinite, bohmite, amorphous silica, etc., these phases will not precipitate at the fluid-mineral interface. However, in natural systems supersaturation of the solutions is likely and will result in the precipitation of secondary minerals. This appears to have occurred in the altered plagioclase at Katmai. The zoned sequence of phases can be interpreted as resulting from the formation of a leached surface layer, followed by precipitation of secondary phases as species are released at the reaction interface and supersaturation occurs. A low pH (1–2), the rate of albite dissolution is increased because the ratio of the activities of alkali cations to protons is small (Helgeson, 1971), and the rapid release of Si and Al causes supersaturation. In sample 212L, Al and Si released from the feldspar have precipitated as smectite and amorphous aluminosilicate in a

layer adjacent to the leached layer. The precipitation of amorphous aluminosilicates and silica during the alteration of Katmai plagioclase is consistent with experimental results at low pH. For example, Yang and Kirkpatrick (1989) have shown that at pH 1–2 aqueous alteration of albite at 250 °C produces kaolinite and amorphous silica, whereas at pH 3–4.5 kaolinite and amorphous aluminosilicate form. The evidence that smectite and amorphous aluminosilicate are only present immediately adjacent to the reaction interface indicates that they are metastable. As the reaction proceeds, aluminosilicates are progressively dissolved because the $Al(OH)_3$ sheets in the clay structure are unstable in acids compared with the silicate sheet (Casey and Bunker, 1990). Close to the fumarole vent, in sample 212J, smectite has not precipitated, but amorphous aluminosilicate has. This difference may be the result of the higher temperature, and subsequent higher solubility of Al in solution closer to the vent, which inhibits supersaturation. In addition, more albitic feldspar is altered closest to the fumarole vent; hence the concentration of Al released into the fluid phase will be lower. Alternatively, it may be that the rate of fluid flow through samples closer to the fumarole was higher, and supersaturation did not occur because of local variations in the permeability of the sample.

Replacement of plagioclase in this study occurred at constant volume, involving the influx of SiO_2-bearing fluids and precipitation of amorphous silica, as indicated by the increase in bulk silica in the protolith material as the fumarole vent is approached. Since the solubility of silica in aqueous fluids is a strong function of temperature, as hot fumarolic fluids infiltrated cooler wall rocks, supersaturation and precipitation of amorphous silica would have occurred. Thus replacement of plagioclase involved SiO_2 from the altering feldspar as well as precipitated silica.

The low concentration of Ca and Na in the leached surface layer indicates that they are rapidly removed from the interface, but probably not as chloride complexes. Experimental data indicate that $CaCl_2$ is increasingly dissociated at temperatures up to about 450–500 °C (Helgeson, 1974), and so Ca may be removed from this system as a dissociated species in H_2O-rich vapor. Likewise Na is probably also removed as a vapor, whereas H_4SiO_4 remains in the reaction zone as amorphous silica. It is also evident from AEM studies that Al is continually leached from the system, as little or no Al is present within the central amorphous region in the alteration zone. The Al is not complexed with Cl (neither Al^{3+} or Si^{4+} forms chloride complexes to any significant degree at either high or low temperatures) and remains as Al^{3+} at low pH (Helgeson, 1974), apparently being removed from the system as a species in the H_2O-rich vapor. A hydrated aluminum hydroxy-fluoride (AHF) has been reported by Keith (1982, 1983) in several Katmai fumaroles and was observed in XRD patterns in the upper portion of this fumarole (Papike et al., 1991b). The presence of the AHF may indicate that Al is being complexed by F and carried

to the surface, where it precipitates at cooler temperatures.

TEM data from the feldspar phenocrysts provide insights into the dynamics of the fumarole system. The data from plagioclase phenocrysts in sample 212J suggest that the influx of fluids into the protolith adjacent to the fumarole vent may have been episodic and possibly cyclic. For example, in the alteration zone in plagioclase shown in Figure 7B, it is clear that there are two distinct generations of alteration, consisting of an early zonal sequence overgrown by a later, more extensive zone of replacement. A possible interpretation of this texture is that the alteration initially proceeded for a period of time when the rock was saturated with fluid. It then appears that the reaction was arrested, probably as a result of the rock drying out. Following this hiatus, fluid must have been reintroduced into the rock, and alteration continued, but the early zoned reaction sequence was preserved. It is conceivable that this hiatus represents a period when the fumarole actually went dormant, but reactivated later.

In addition to the evidence that there may have been major periods of inactivity in the fumarole, there are also textural indicators of shorter term, cyclic fluctuations in fluid influx. This can be best seen in Figures 7A, 7B, and 9C in the form of narrow, concentric zones in the regions of alteration in plagioclase, which are visible in the amorphous silica. One interpretation of this type of feature is that it represents short-term fluctuations in fluid flow, which might have occurred on a seasonal basis. For example, the rate of circulation of meteoric H_2O would have been much higher in the late spring and early summer, when run-off from the melting snow pack was high, but it would have tailed off over the fall and winter.

Alteration of augite

Although the alteration mechanism of augite is similar to that for plagioclase, there are some important differences. The zonal sequence at the augite interface can also be interpreted as a leached surface layer, followed by a zone of secondary precipitates, and finally amorphous silica precipitated from the fumarolic fluids. The leached zone is depleted in MgO and CaO, which are readily removed from the surface in solution, but FeO and SiO_2 are enhanced. Experimental studies at 20–75 °C indicate that diopside exhibits incongruent dissolution behavior (Schott et al., 1981) at an early stage in the dissolution reaction but reaches a steady state, where the dissolution becomes congruent. At low pH, a leached layer develops, with Ca and Mg being preferentially removed, and a silica-rich layer forms at the surface. The thickness of the surface layer that develops in experimental studies appears to be controversial. For example, Schott et al. (1981) suggested that the leached layer is probably on the order of 200 Å, but Petit et al. (1987) reported penetration of H as much as 1000 Å into reacting diopside. The thickness of the leached zone observed in augite at Katmai is approximately 200–300 Å and is consistent with the experimental results reported above.

Unlike altered plagioclase in the same sample, secondary precipitation of halloysite has occurred. However, it is clear that the halloysite is progressively dissolved and replaced by amorphous silica from the fumarolic fluids. In addition, the chemistry of the leached layer in augite differs from that in plagioclase by lacking high concentrations of Cl. It is not obvious why such differences should exist. Local differences in the pH of the solution great enough that absorption of Cl into the surface layer would not be favored is one possibility. Although it is difficult to envision a scenario where that could occur, such a variation might account for the precipitation of halloysite as a breakdown product of augite, but not of plagioclase, in the same sample. Al released from the breakdown of augite was clearly not removed in solution, but it has been concentrated at the surface of the leached layer, since the Al_2O_3 content of augite is only on the order of 1–2 wt%. This contrasts sharply with plagioclase, where Al was clearly removed very rapidly. This variation may be the result of contrasting rates of fluid flow through different regions of the sample, as has been noted by Hochella et al. (1988). They found that halloysite was distributed very heterogeneously through their experimental core, in which aqueous fluid was flowing through the sample. They attributed this phenomenon to local, slower flow rates through pores and the possibility of supersaturation and precipitation occurring.

CONCLUSIONS

Perhaps one of the major observations in this study is that the processes of feldspar and pyroxene dissolution in a highly acidic, natural environment are entirely consistent with experimental studies of feldspar alteration under low pH conditions. In particular, we have observed the presence of a leached surface layer in feldspar that is enriched in Cl, a phenomenon that has only been previously observed in experimental studies carried out under conditions of low pH. The thicknesses of leached surface layers found in altering feldspar (and pyroxene) observed directly by TEM techniques are also comparable with those produced experimentally. Finally, this study illustrates that even in extremely complex geological systems, such as fumaroles, it is possible to unravel the mechanisms of mineral-fluid reactions involving specific mineral phases, which ultimately control elemental mass transport on the larger scale. These observations, combined with our previous bulk chemical studies, provide a powerful approach to understanding and interpreting fumarolic systems.

REFERENCES CITED

Ahn, J.H., and Peacor, D.R. (1986) Transmission and analytical electron microscopy of the smectite to illite transition. Clays and Clay Minerals, 34, 165–170.

Allen, E.T., and Zies, E.G. (1923) A chemical study of fumaroles of the Katmai region. National Geographic Society, Contributed Technical Papers, Katmai Series, 2, 75–155.

Banfield, J.F., and Eggleton, R.A. (1990) Analytical transmission electron microscope studies of plagioclase, muscovite and K-feldspar weathering. Clays and Clay Minerals, 38, 77–89.

Bence, A.E., and Albee, A.L. (1968) Empirical correction factors for the electron microanalysis of silicates and oxides. Journal of Geology, 76, 382–403.

Casey, W.H., and Bunker, B. (1990) Leaching of mineral and glass surfaces during dissolution. Mineralogical Society of America Reviews in Mineralogy, 23, 397–426.

Casey, W.H., Westrich, H.R., Arnold, G.W., and Banfield, J.F. (1989) The surface chemistry of dissolving labradoritic feldspar. Geochimica et Cosmochimica Acta, 53, 821–832.

Casey, W.H., Westrich, H.R., and Holdren, G.R. (1991) Dissolution rates of plagioclase at pH = 2 and 3. American Mineralogist, 76, 211–217.

Chou, L., and Wollast, R. (1985) Steady-state kinetics and dissolution mechanisms of albite. American Journal of Science, 285, 963–993.

Cliff, G., and Lorimer, G.W. (1975) Quantitative analysis of thin specimens. Journal of Microscopy, 103, 203–207.

Eggleton, R.A., and Buseck, P.R. (1980) High resolution electron microscopy of feldspar weathering. Clays and Clay Minerals, 28, 173–178.

Grant, J.A. (1986) The isocon diagram: A simple solution to Gresens' equation for metasomatic alteration. Economic Geology, 81, 1976–1982.

Guthrie, G.D., and Veblen, D.R. (1990) Interpreting one-dimensional high resolution transmission electron micrographs of sheet silicates by computer simulation. American Mineralogist, 75, 276–288.

Helgeson, H.C. (1971) Kinetics of mass transport among silicates and aqueous solutions. Geochimica et Cosmochimica Acta, 35, 421–469.
——— (1974) Chemical interaction of feldspars and aqueous solutions. In W.S. Mackenzie and J. Zussman, Eds., Proceedings of NATO advance study institute, p. 184–217. Manchester University Press, Manchester, U.K.

Hellmann, R., Eggleston, C.M., Hochella, M.F., Jr., and Crerar, D.A. (1990) The formation of leached layers on albite surfaces during dissolution under hydrothermal conditions. Geochimica et Cosmochimica Acta, 54, 1267–1282.

Hildreth, W. (1983) The compositionally zoned eruption of 1912 in the Valley of Ten Thousand Smokes, Katmai National Park, Alaska. Journal of Volcanic and Geothermal Research, 18, 1–56.

Hochella, M.F., Jr., Ponader, H.B., Turner, A.M., and Harris, D.W. (1988) The complexity of mineral dissolution as viewed by high resolution Auger microscopy: Labradorite under hydrothermal conditions. Geochimica et Cosmochimica Acta, 52, 385–394.

Holdren, G.R., Jr., and Berner, R.A. (1979) Mechanism of feldspar weathering. I. Experimental studies. Geochimica et Cosmochimica Acta, 43, 1161–1171.

Hurst, V.J., and Kunkle, A.C. (1985) Dehydroxylation, rehydration, and stability of kaolinite. Clays and Clay Minerals, 33, 1–14.

Jarosewich, E., Nelen, J.A., and Norberg, J.A. (1980) Reference samples for electron microprobe analysis. Geostandards Newsletter, 4, 43–47.

Keith, T.E.C. (1982) Preliminary observations on fumarole distribution and alteration, Valley of Ten Thousand Smokes, Alaska. In K.M. Reed and S. Bartsch-Winkler, Eds., The United States Geological Survey in Alaska: Accomplishments during 1982. U.S. Geological Survey Circular, 939, 82–85.
——— (1983) Mineralogical and chemical changes in fumarolic deposits with time at surface conditions. International Symposium on Water-Rock Interaction, Proceedings, Misasa, Japan, 4, 231–234.
——— (1984) Preliminary observations on fumarole distribution and alteration, Valley of 10,000 Smokes, Alaska. U.S. Geological Survey Circular, 939, 82–85.
——— (1985) Active hydrothermal alteration in the vicinity of the Novarupta dome, Valley of 10,000 Smokes, Alaska. Transactions of the American Geophysical Union, 46, 1154.

——— (1991a) Fossil and active fumaroles in the 1912 eruptive deposits, Valley of Ten Thousand Smokes, Alaska. Journal of Volcanic and Geothermal Research, 45, 227–254.
——— (1991b) Argillic alteration in the Novarupta vent region, Katmai National Park, Alaska. Geophysical Research Letters, 18, 1549–1552.

Kienle, J. (1991) Depth of the ash flow deposit in the Valley of Ten Thousand Smokes, Katmai National Park, Alaska. Geophysical Research Letters, 18, 1533–1536.

Klimentidis, R.E., and Mackinnon, I.D.R. (1986) High resolution imaging of ordered mixed-layer clays. Clays and Clay Minerals, 34, 155–164.

Kodosky, L., and Keskinen, M. (1990) Fumarole distribution, morphology, and encrustation mineralogy associated with the 1986 eruptive deposits of Mount St. Augustine, Alaska. Bulletin of Volcanology, 52, 175–185.

Lovering, T.S. (1957) Halogen-acid alteration of ash at Fumarole No. 1, Valley of Ten Thousand Smokes, Alaska. Geological Society of America Bulletin, 68, 1585–1604.

Mackinnon, I.D.R., Lumpkin, G.R., and Van Deusen, S.B. (1986) Thin-film analyses of silicate standards at 200kV: The effect of temperature on element loss. In A.D. Romig and W.F. Chambers, Eds., Microbeam analysis—1986, p. 451–454. San Francisco Press, San Francisco, California.

Muir, I.J., Bancroft, G.M., and Nesbitt, H.W. (1989) Characteristics of altered labradorite surfaces by SIMS and XPS. Geochimica et Cosmochimica Acta, 53, 1235–1241.

Newman, A.C.D., and Brown, G. (1987) The chemical composition of clays. In A.C.D. Newman, Ed., Chemistry of clays and clay minerals: Mineralogical Society monograph 6, 480 p. Longman's, London.

Papike, J.J. (1992) The Valley of Ten Thousand Smokes, Katmai, Alaska: A unique geochemistry laboratory. Geochimica et Cosmochimica Acta, 56, 1429–1449.

Papike, J.J., Keith, T.E.C., Spilde, M.N., Shearer, C.K., Galbreath, K.C., and Laul, J.C. (1991a) Major and trace element mass flux in fumarolic deposits, Valley of Ten Thousand Smokes, Alaska: Rhyolite-rich protolith. Geophysical Research Letters, 18, 1545–1548.

Papike, J.J., Keith, T.E.C., Spilde, M.N., Galbreath, K.C., Shearer, C.K., and Laul, J.C. (1991b) Geochemistry and mineralogy of fumarolic deposits, Valley of Ten Thousand Smokes, Alaska: Bulk chemical and mineralogical evolution of dacite-rich protolith. American Mineralogist, 76, 1662–1673.

Petit, J.-C., Mea, G.D., Dran, J.-C., Schott, J., and Berner, R.A. (1987) Mechanism of diopside dissolution from hydrogen depth profiling. Nature, 325, 705–707.

Schott, J., Berner, R.A., and Sjöberg, E.L. (1981) Mechanism of pyroxene and amphibole weathering. I. Experimental studies of iron-free minerals. Geochimica et Cosmochimica Acta, 45, 2123–2135.

Shipley, J.W. (1920) Some chemical observations on the volcanic emanations and incrustations in the Valley of 10,000 Smokes, Katmai, Alaska. American Journal of Science, 50, 141–153.

Symonds, R.B., Rose, W.I., Reed, M.H., Lichte, F.E., and Finnegan, D.L. (1987) Volatilization, transport and sublimation of metallic and nonmetallic elements in high temperature gases at Merapi Volcano, Indonesia. Geochimica et Cosmochimica Acta, 51, 2083–2101.

Tazaki, K. (1982) Analytical electron microscopic studies of halloysite formation processes: Morphology and composition of halloysite. In Proceedings, International Clay Conference 1981, Italy, p. 573–584. Elsevier, Amsterdam.

Velde, D., and Meunier, A. (1987) Petrologic phase equilibria in natural clay systems. In A.C.D Newman, Ed., Chemistry of clays and clay minerals, Mineralogical Society monograph 6, p. 423–458. Longman's, London.

Yang, W.-H.A., and Kirkpatrick, R.J. (1989) Hydrothermal reaction of albite and a sodium aluminosilicate glass: A solid-state NMR study. Geochimica et Cosmochimica Acta, 53, 805–819.

Zies, E.G. (1929) The Valley of Ten Thousand Smokes. I. The fumarolic incrustations and their bearing on ore deposition. II. The acid gases contributed to the sea during volcanic activity. National Geographic Society, Contributed Technical Papers, Katmai Series, 4, 1–79.